

Effect of Lewis acid-base additive on lead-free Cs_2SnI_6 thin film prepared by direct solution coating process

Saqib Nawaz Khan, Yan Wang(王燕), Lixiang Zhong(钟李祥), Huili Liang(梁会力), Xiaolong Du(杜小龙), and Zengxia Mei(梅增霞)

Citation: Chin. Phys. B, 2024, 33 (**8**): 087201. DOI: 10.1088/1674-1056/ad4a39

What follows is a list of articles you may be interested in

Impacts of hydrogen annealing on the carrier lifetimes in p-type 4H-SiC after thermal oxidation

Ruijun Zhang(张锐军), Rongdun Hong(洪荣墩), Jingrui Han(韩景瑞), Hungkit Ting(丁雄杰), Xiguang Li(李锡光), Jiafa Cai(蔡加法), Xiaping Chen(陈厦平), Deyi Fu(傅德颐), Dingqu Lin(林鼎渠), Mingkun Zhang(张明昆), Shaoxiong Wu(吴少雄),Yuning Zhang(张宇宁), Zhengyun Wu(吴正云), and Feng Zhang(张峰)
Chin. Phys. B, 2023, 32 (**6**): 067205. DOI: 10.1088/1674-1056/ac89db

Enhanced thermoelectric properties of p-type polycrystalline SnSe by regulating the anisotropic crystal growth and Sn vacancy

Chengyan Liu(刘呈燕), Lei Miao(苗蕾), Xiaoyang Wang(王潇漾), Shaohai Wu(伍少海), Yanyan Zheng(郑岩岩), Ziyang Deng(邓梓阳), Yulian Chen(陈玉莲), Guiwen Wang(王桂文), Xiaoyuan Zhou(周小元)
Chin. Phys. B, 2018, 27 (**4**): 047211. DOI: 10.1088/1674-1056/27/4/047211

Al-doping influence on crystal growth of Ni-Al alloy: Experimental testing of a theoretical model

Rong Xi-Ming (荣曦明), Chen Jun (陈骏), Li Jing-Tian (李菁田), Zhuang Jun (庄军), Ning Xi-Jing (宁西京)
Chin. Phys. B, 2015, 24 (**12**): 128706. DOI: 10.1088/1674-1056/24/12/128706

Colloidal monolayer self-assembly and its simulation via cellular automaton model

Wu Yi-Zhi (吴以治), Chen Chen (陈晨), Xu Xiao-Liang (许小亮), Liu Yun-Xi (刘赟夕), Shao Wei-Jia (邵伟佳), Yin Nai-Qiang (尹乃强), Zhang Wen-Ting (张文婷), Ke Jia-Xin (柯佳鑫), Fang Xiao-Tian (方啸天)
Chin. Phys. B, 2014, 23 (**8**): 088703. DOI: 10.1088/1674-1056/23/8/088703

Effect of Lewis acid-base additive on lead-free Cs_2SnI_6 thin film prepared by direct solution coating process

Saqib Nawaz Khan[1,2,3], Yan Wang(王燕)[4], Lixiang Zhong(钟李祥)[5], Huili Liang(梁会力)[1,2], Xiaolong Du(杜小龙)[1,2,3], and Zengxia Mei(梅增霞)[1,2,†]

[1] *Institute of Physics, Chinese Academy of Sciences, Beijing* 100190, *China*
[2] *Songshan Lake Materials Laboratory, Dongguan* 523808, *China*
[3] *University of Chinese Academy of Sciences, Beijing* 100049, *China*
[4] *Beijing Hairou Laboratory, Beijing* 101400, *China*
[5] *School of Physics, Beijing Institute of Technology, Beijing* 100081, *China*

(Received 1 March 2024; revised manuscript received 30 April 2024; accepted manuscript online 13 May 2024)

Inorganic Cs_2SnI_6 perovskite has exhibited substantial potential for light harvesting due to its exceptional optoelectronic properties and remarkable stability in ambient conditions. The charge transport characteristics within perovskite films are subject to modulation by various factors, including crystalline orientation, morphology, and crystalline quality. Achieving preferred crystalline orientation and film morphology via a solution-based process is challenging for Cs_2SnI_6 films. In this work, we employed thiourea as an additive to optimize crystal orientation, enhance film morphology, promote crystallization, and achieve phase purity. Thiourea lowers the surface energy of the (222) plane along the ⟨111⟩ direction, confirmed by x-ray diffraction, x-ray photoelectron spectroscopy, ultraviolet photoelectron spectroscopy studies, and density functional theory calculations. Varying thiourea concentration enables a bandgap tuning of Cs_2SnI_6 from 1.52 eV to 1.07 eV. This approach provides a novel method for utilizing Cs_2SnI_6 films in high-performance optoelectronic devices.

Keywords: Cs_2SnI_6, crystalline orientation, Lewis acid-case, additive engineering, bandgap engineering

PACS: 72.80.Jc, 87.15.nt, 91.60.Ed, 68.55.–a **DOI:** 10.1088/1674-1056/ad4a39

1. Introduction

Low-cost fabrication, ease of processing, and excellent light harvesting properties make Cs_2SnI_6 perovskite a compelling contender among the most competitive candidates for applications in optoelectronic devices. The non-toxic lead-free and highly stable inorganic Cs_2SnI_6 perovskite got considerable attention due to its outstanding optoelectronic properties such as high absorption coefficient, ambipolar transport, high carrier mobility, long diffusion length, flexible bandgap adjustment, etc.[1–5] This makes Cs_2SnI_6 perovskite an attractive choice for applications in various devices such as solar cells, detectors, light-emitting diodes, and field effect transistors.[6–12]

Cs_2SnI_6 perovskite films have been fabricated through various methods, including hydrothermal process, hot injection, and spin coating.[7,9,13–17] However, the corresponding device performance falls significantly below the reported material properties. Further optimization and in-depth studies are deemed necessary to enhance device performance by optimizing Cs_2SnI_6 thin film quality and fully exploring the potential of Cs_2SnI_6 perovskite films. Compared to other fabrication methods, spin coating is a low-cost and fast fabrication route, allowing flexible control over film composition and optoelectronic properties. In the spin coating process for perovskite film formation, early crystallization dynamics play a crucial role in determining the film's quality and performance. This phenomenon is influenced by factors such as the solution composition and process parameters.[18,19] The implications include non-uniform crystalline structures and reduced optoelectronic properties. Several strategies have been explored to address this challenge, such as optimization of nucleation and annealing, intermittent spin-coating method, anti-solvent crystallization strategies, and additive engineering.[20,21] Thiourea consists of two amino groups and one S-donor which naturally benefits additive engineering. It has been widely utilized as an additive in lead-based perovskite materials to enhance their crystallization properties including orientation, morphology, and grain size.[22–25] DFT study shows that Cs_2SnI_6 crystal orientation along different surfaces has different thermodynamic stability and indicates high thermodynamic stability along ⟨111⟩ plane direction.[26] So far, however, thiourea hasn't been adopted as an additive in Cs_2SnI_6 double perovskite yet, not to mention its effects on the material's crystalline orientation.

We realized crystalline orientation-controllable Cs_2SnI_6 film growth by one-step spin coating method via thiourea engineering. By combining x-ray diffraction (XRD), x-ray photoelectron spectroscopy (XPS), and ultraviolet photoelectron spectroscopy (UPS), we found that thiourea significantly enhances a crystalline orientation along ⟨111⟩ direction. Besides, high crystallization quality and good mor-

†Corresponding author. E-mail: zxmei@iphy.ac.cn

© 2024 Chinese Physical Society and IOP Publishing Ltd

phology were achieved along with a high absorption coefficient of 8.8×10^4 cm^{-1}. Additionally, DFT analysis revealed that a higher absorption energy (-0.716 eV) of thiourea at (222) plane compared to the one at (400) plane (-0.679 eV) greatly stabilizes the (222) plane. Varying thiourea concentration enables a bandgap tuning of Cs_2SnI_6 from 1.52 eV to 1.07 eV. These findings highlight the significance of controlling the crystalline orientation and tuning the optical properties of Cs_2SnI_6 thin films through thiourea, which may enable a new strategy for low-cost and lead-free Cs_2SnI_6-based optoelectronic devices.

2. Computational and experimental details

2.1. First-principles density functional theory computation

First-principles calculations were carried out using the density functional theory (DFT) method as implemented in the Vienna *ab initio* simulation package (VASP).[27] The ion–electron interactions were treated with the projected augmented wave pseudopotentials,[28] and the general gradient approximation (GGA) with the Perdew–Burke–Ernzerhof functional was used to describe the exchange–correlation potential when performing geometric relaxation.[29] The plane-wave basis was expanded up to a cut-off energy of 400 eV. All structures were relaxed using a conjugate gradient method until the residual force on every atom was less than 0.01 eV/Å, and the convergence criteria of total energy in the self-consistent field method were set to 10^{-5} eV. The DFT-D3 method of Grimme *et al.*[30] was adopted to take into account vdW-dispersion energy correction. The adsorption energy (E_{ads}) was defined as $E_{ads} = E_{total} - E_{substrate} - E_{adsorbate}$, where E_{total}, $E_{substrate}$, and $E_{adsorbate}$ are the energy of the total system, pristine substrate, and isolated adsorbate, respectively. A negative E_{ads} indicates energy decline upon adsorption and a more negative E_{ads} value means a stronger adsorption.

2.2. Materials

Cesium iodide (analytical grade (AR), 98%), tin (IV) iodide (99.95%), thiourea (99%), N, N dimethyl-formamide (DMF) (99.5%), and chlorobenzene were purchased from Shanghai Macklin Biochemical Co. Ltd. Dimethyl-sulfoxide (DMSO) (AR, $>$ 99%) was purchased from Alfa Aesar and Aladin Biochemical Technology Co. Ltd, respectively. All chemicals were used directly without further purification.

2.3. Cs_2SnI_6 thin film fabrication

The Cs_2SnI_6 precursor was prepared by dissolving cesium iodide (1 mmol) and tin iodide (1 mmol) in a mixing solvent consisting of DMSO (0.9 ml) and DMSO (0.4 ml) under magnetic stirring. Different amounts of thiourea (0 mmol, 0.14 mmol, 0.28 mmol, 0.42 mmol, 0.56 mmol, and 0.7 mmol represented by samples S_0, S_1, S_2, S_3, S_4, and S_5, respectively) were added to the prepared solution. The obtained solution was filtered with a 450 nm filter before spin coating.

Glass substrate with a total thickness of 2 mm was subsequentially cleaned with acetone, ethanol, and deionized water for 15 min at 50 °C followed by ultraviolet treatment. The Cs_2SnI_6 precursor solution was spin-coated on the cleaned glass substrate at 1000 rpm for 10 s, then 2500 rpm for 40 s, using chlorobenzene as an anti-solvent during the last 30 s. The obtained film was followed by pre-annealing at 40 °C for 1 min in the glovebox and crystallized at 150 °C for 2 min on a hot plate in the air.

2.4. Characterization

Powder x-ray diffraction (D8-ADVANCE) using Cu $K\alpha$ radiation was used to characterize the crystal structures of the Cs_2SnI_6 films. Field-emission scanning electron microscopy (Hitachi Regulus 8100) was used to measure the film morphology. The surface roughness of the Cs_2SnI_6 films was obtained by AFM (Cypher S/Oxford Instruments Asylum Research). X-ray photoelectron spectroscopy and ultraviolet photoelectron spectroscopy (Thermo Fisher ESCALAB XI+) determined the valance state of the constituents and work function of the Cs_2SnI_6 films. UV–Vis–NIR absorbance spectrums of Cs_2SnI_6 films were conducted using HATACHI UH4150.

3. Results and discussion

To get insight into the crystal structure, the out-of-plane x-ray diffraction (XRD) of Cs_2SnI_6 films was performed. XRD curves of all Cs_2SnI_6 films prepared with varied amounts of thiourea represented by S_0–S_5 are shown in Fig. 1(a). Characteristic peaks of all the samples were found located at 13.1°, 26.5°, and 30.7° which can be assigned to the (111), (222), and (400) planes of the Cs_2SnI_6 crystal, respectively. However, no characteristic peak of thiourea is found indicating that thiourea did not incorporate into the Cs_2SnI_6 films. The characteristic peaks of Cs_2SnI_6 in sample S_0 are weaker while one intense peak corresponding to the (110) plane of CsI appears at 27.6°. Furthermore, a nearly linear drop in the intensity ratio of (400)/(222) peaks is observed from S_0 to S_3. Importantly, sample S_3 shows the highest peak intensity of the (222) plane compared to sample S_0 prepared without thiourea or those employing other different thiourea concentrations. Simultaneously, it shows almost zero intensity of (400) and (440) planes without CsI impurity peaks, which shows that the film prefers to grow along the (222) direction rather than in other directions after the appropriate addition of thiourea. It could be attributed to the Lewis acid-base adduct effect which promotes the growth of Cs_2SnI_6 crystal along the (222) plane and results in pure single plane orientation of crystal along $\langle 111 \rangle$ direction relative to the substrate.

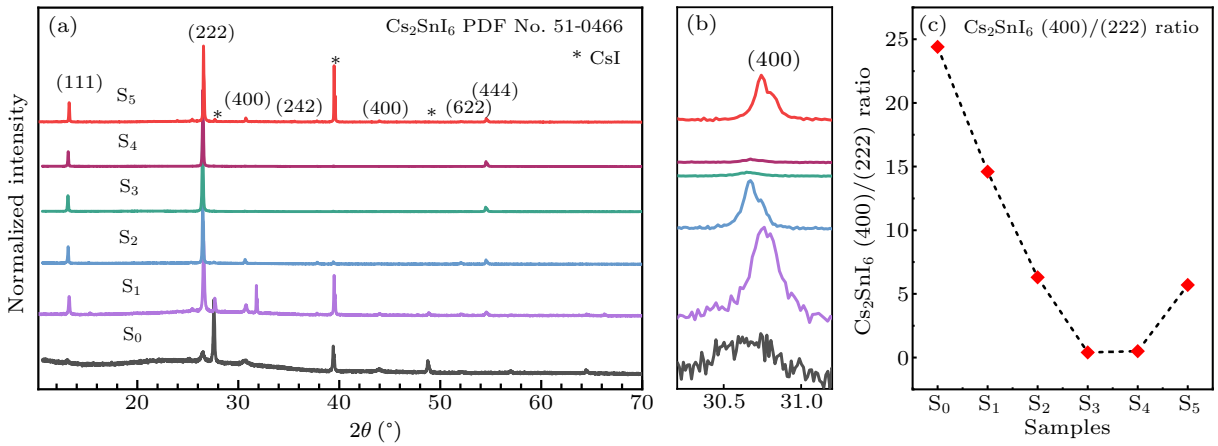


Fig. 1. (a) XRD pattern (b) peaks of (400) plane and (c) ratio of (400)/(222) plane of Cs_2SnI_6 thin film prepared with varying amounts of thiourea represented by S_0–S_5.

DFT calculations were used to verify the capability of thiourea molecules to alter the crystalline orientation of Cs_2SnI_6 perovskite. The most stable configurations are shown in Fig. 2(a), which depicts the interactions between thiourea and Cs_2SnI_6. The sulfur atom in the thiourea molecule interacts with Sn^{4+} of Cs_2SnI_6 perovskite through a coordination bond, and the hydrogen atoms interact with I by the hydrogen bond. The adsorption of thiourea on the {100} surface (−0.679 eV) is found to be weaker than on the {111} surface (−0.716 eV), indicating the further stabilization of {111} surface and decreasing the {100}/{111} ratio. The stronger adsorption of thiourea on the {111} surface is due to more hydrogen atoms pointing to the surface as compared to the {100} surface.

The impact of thiourea on the crystalline orientation of the resulting Cs_2SnI_6 thin film can be schematically illustrated in Fig. 2(b). The main component of the film prepared without thiourea in precursor solution is CsI, with only a small amount of Cs_2SnI_6 present. Upon the appropriate addition of thiourea to the solution, the film comes out Cs_2SnI_6 with a distinct crystalline orientation of (222). The variation in film composition between the samples prepared with and without thiourea can be attributed to the multifaceted role of thiourea in influencing the crystallization process and crystal orientation during film formation. Firstly, thiourea, with its unique chemical structure containing sulfur and amine groups, interacts with the CsI/SnI_4 species and the crystal surfaces in the precursor solution. This interaction alters the surface energy of the crystal facets, thereby affecting the kinetics of crystal growth and the preferential adsorption of thiourea on specific crystal facets. Moreover, thiourea modifies the nucleation and growth kinetics of Cs_2SnI_6 crystals during film formation, promoting the growth of Cs_2SnI_6 over CsI. By altering the crystal growth dynamics, thiourea facilitates the formation of Cs_2SnI_6 films instead of CsI-dominant films. Besides, the observed variation in crystalline orientation can be attributed to the relative adsorption intensity of thiourea on the {100}, {111} surfaces and the intricate relationship between thiourea concentration and its interaction with crystal surface passivation and crystal growth dynamics.

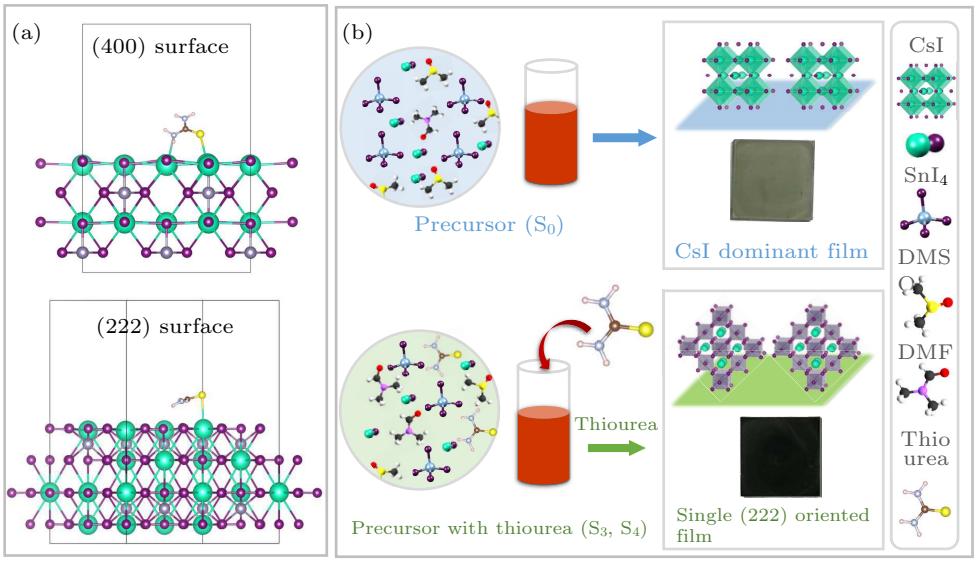


Fig. 2. (a) Schematic illustration of the interaction between (400) and (222) surfaces of perovskite and thiourea. (b) Schematic of additive engineering by thiourea, the mixed crystalline orientation of the resulting Cs_2SnI_6 film without thiourea (top) and single crystalline orientation following the introduction of thiourea (bottom), the inset shows the photographic images of Cs_2SnI_6 thin films prepared with and without thiourea.

At the optimized thiourea concentration (S_3, S_4), there is a balance between the number of thiourea molecules available for interaction and the surface area of the crystal, leading to a specific effect on the crystalline orientation. This concentration may facilitate a more pronounced interaction between thiourea molecules and the crystal surfaces, resulting in the preferential adsorption or passivation of certain crystal facets, such as the (400) plane. As a result, the (400) plane is eliminated, while the (222) plane remains intact. Conversely, at concentrations lower or higher than optimal concentration, the balance between thiourea molecules and crystal surfaces may shift, leading to different effects on the crystalline orientation. At lower thiourea concentrations, there may not be enough thiourea molecules available to sufficiently interact with the crystal surfaces. This insufficient interaction leads to less pronounced effects on crystalline orientation, resulting in the presence of both the (400) and (222) planes. Similarly, at higher concentrations, an excess of thiourea molecules may lead to more pronounced interactions between the additive and the Cs_2SnI_6 crystal surface. This could potentially result in the preferential adsorption of thiourea on specific crystal facets, altering their surface energy and influencing crystal growth kinetics.[31] Under certain conditions, this selective adsorption may favor the formation of the (400) plane. Additionally, the formation of complexes between thiourea and tin ions on the crystal surface may also modulate crystal growth behavior. As the concentration of thiourea increases, more complexation sites become available on the crystal surface, potentially facilitating the nucleation and growth of previously suppressed crystal planes, ultimately resulting in the presence of both the (222) and (400) planes. Overall, the presence of thiourea in the precursor solution exerts a comprehensive influence on the crystallization process, promoting the formation of Cs_2SnI_6 films with improved composition and properties compared to films prepared without thiourea.

Figure 3 shows the surface morphology of Cs_2SnI_6 film prepared with different amounts of thiourea concentration represented by S_0–S_5. A huge difference is observed in film morphology subjected to varied amounts of thiourea. Specifically, the film prepared without thiourea S_0 and those incorporating a low amount of thiourea S_1 exhibit suboptimal surface coverage and the presence of voids. Nonetheless, an incremental improvement in film morphology is discernible with each successive increase in thiourea concentration. A significant improvement in film surface morphology is observed with compact, dense, and continuous film using 0.42 mmol (S_3) of thiourea concentration. Further increasing the amount of thiourea to 0.7 mmol (S_5) results in voids and low coverage. The improved morphology could be attributed to the regulated nucleation process and cross-linker effect due to the Lewis acid-base adduct of the thiourea molecule. The Lewis acid-base adduct could be formed between the S atom and tin halides while H-bonding between the amine group and CsI, promoting the interaction of CsI into Sn halides to form perovskite nucleus. Conversely, a higher amount of thiourea leads CsI to form large aggregates, inhibiting the interaction between CsI and Sn halides which results in lower coverage and poor morphology. To sum up, an optimal amount of thiourea concentration serves to catalyze the creation of dense and uniform perovskite nuclei, thereby yielding an ameliorated film morphology.

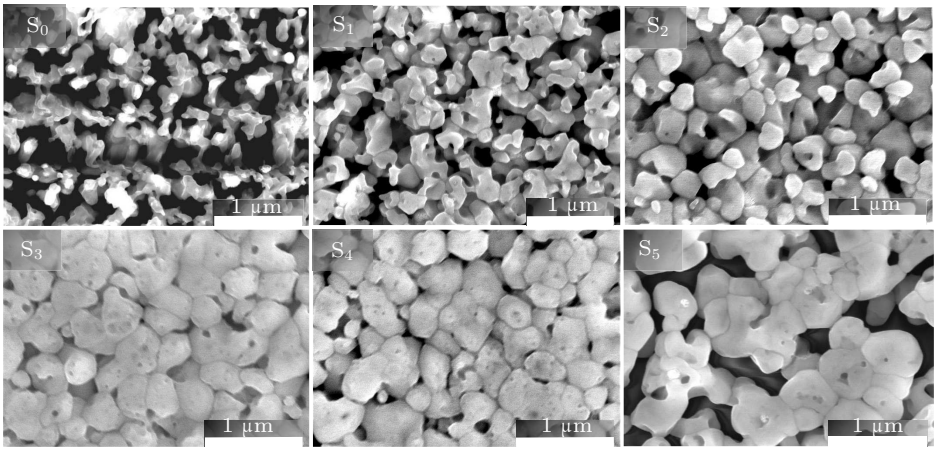


Fig. 3. SEM images of Cs_2SnI_6 thin film prepared with different amounts of thiourea concentration, labeled as samples S_0–S_5, corresponding to 0 mmol, 0.14 mmol, 0.28 mmol, 0.42 mmol, 0.56 mmol, and 0.7 mmol, respectively.

To further investigate the effect of thiourea on surface roughness and surface current characteristics, AFM and conductive-AFM (C-AFM) were carried out as shown in Fig. 4. The surface roughness of the film prepared without thiourea differs a lot from the films prepared with thiourea consistent with SEM analysis. A small cluster is observed on the surface of S_0 and S_1 while the other samples show larger grains with clear grain boundaries, indicating that adding a sufficient amount of thiourea can improve the crystallinity of Cs_2SnI_6. The AFM results demonstrate comparable surface

roughness for samples S_1–S_3. A slight elevation in roughness is observed in S_4, whereas the highest surface roughness is evident in samples S_0 and S_5. The C-AFM was carried out to analyze the surface conductivity properties of Cs_2SnI_6 thin films of S_0–S_5. Each scan completes a 3 μm×3 μm area, with a scan rate of 1 Hz. A bias of ±1 V was applied to the tip to measure the local conductivity of the samples. Figure 4(b) shows the C-AFM conductivity map obtained for the samples prepared with varying amounts of thiourea concentration. The data reveals distinct conductivity variations across the sample surface. The sample S_0 prepared without thiourea did not show current variation, with minimal fluctuation for samples S_1 and S_5 under applied voltage. In contrast, samples S_2, S_3, and S_4 exhibited a distinct variation in their current profiles. The sample S_3 shows significantly more and larger high current areas than other samples. It could be ascribed to the enhanced film morphology and crystallization quality of S_3.

To investigate the effect of thiourea on the electronic properties of the resultant film, Hall effect measurement was carried out as shown in Table 1. The sample S_0 does not show a stable value of carrier concentration and mobility. The carrier concentration and mobility increase from 4.536×10^{14} cm^{-3} to 4.095×10^{15} cm^{-3} and 7.078 cm^2/V·s to 366 cm^2/V·s for S_1 to S_3 while the resistivity decreases from 1.944×10^3 to 4.165 respectively. It could be attributed to the improved crystalline quality and surface morphology indicated by XRD, SEM, and CAFM. By further increasing the amount of thiourea shown by S_4, the carrier concatenation and mobility drops again which could be due to poor surface compared to sample S_3.

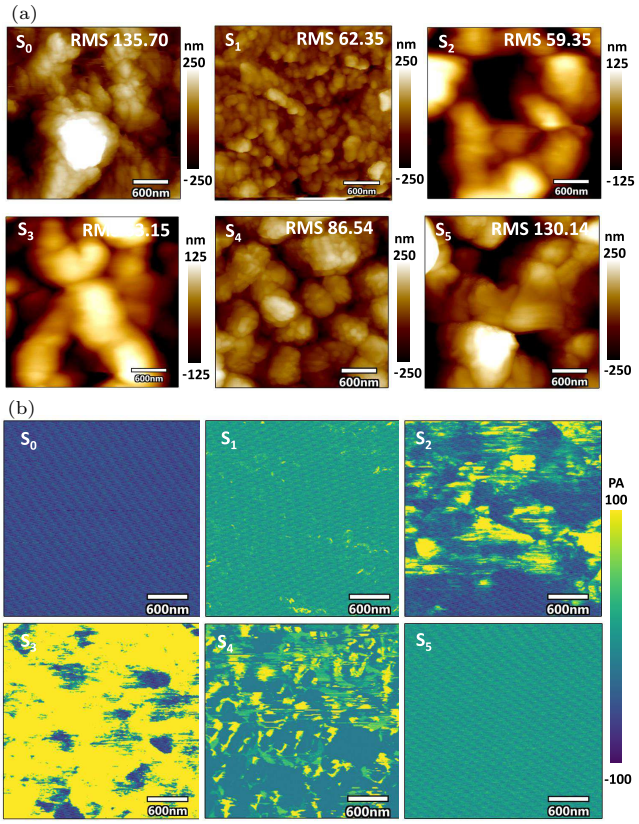


Fig. 4. (a) AFM images and (b) C-AFM mapping images of Cs_2SnI_6 thin film prepared with different amounts of thiourea concentration.

Table 1. The electronic properties obtained from hall effect measurement of Cs_2SnI_6 film prepared with different amounts of thiourea concentration.

Sample	Carrier concentration (cm^{-3})	Mobility (cm^2/V·s)	Resistivity (Ω·cm)	Conductivity (Ω·cm)
S_0	–	–	–	–
S_1	4.536×10^{14}	7.078	1.944×10^3	5.143×10^{-4}
S_2	2.938×10^{15}	86.67	24.51	4.080×10^{-2}
S_3	4.095×10^{15}	366.0	4.165	2.401×10^{-1}
S_4	2.520×10^{13}	352.5	702.9	9.490×10^{-4}
S_5	1.997×10^{13}	3.839	8.141×10^4	1.228×10^{-5}

The effect of thiourea on the optical properties of CSI film deposited on a glass substrate was analyzed by using UV–Vis–NIR spectroscopy. The absorption spectra of samples prepared with different amounts of thiourea represented by S_0–S_5 differ significantly are shown in Fig. 5(a). The absorption coefficient of the samples S_0 and S_1 decreases rapidly when the wavelength increases. In the samples S_2 and S_3, there is significant improvement in absorption spectra above 410 nm to near infrared region. Further increasing thiourea amount (S_4 and S_5) results in lower absorption values in the wavelength region shorter than 800 nm while higher absorption values in longer wavelength regions. Overall, sample S_3 gives the highest absorption coefficient reaching 8.8×10^4 cm^{-1} in the visible range while sample S_5 gives comparatively better absorption in the NIR range. The variation in absorption values over different thiourea concentrations might come from either compositional change leading to a change in bandgap or morphological changes of CSI perovskite in agreement with XRD and SEM analysis. The optical bandgap (E_g) values derived from the Tauc plot, are depicted in Fig. 5(b) illustrating the influence of thiourea concentration. The sample S_0 exhibits an optical bandgap of 1.52 eV. A discernible trend emerges with increasing thiourea concentration, leading to a gradual reduction in optical bandgap. Notably the lowest optical bandgap reaching 1.07 eV is obtained for S_5. The significant impact of thiourea on the bandgap of Cs_2SnI_6 films can be attributed to its role as a surface modifier during the film formation process. Thiourea molecules, with their unique chemical structure con-

taining sulfur and amine groups, can interact with the Cs_2SnI_6 precursor solution and the resulting thin film in several ways. Thiourea can act as a surface passivant by binding to defect sites or dangling bonds on the film surface, effectively reducing non-radiative recombination processes.[32,33] This passivation effect enhances the efficiency of light absorption and emission, potentially leading to a reduction in the band-gap energy.[34] Furthermore, thiourea may influence the nucleation and growth kinetics of Cs_2SnI_6 crystals during film formation, altering the crystal morphology and structure. By modifying the crystal growth rate or promoting the growth of certain crystal facets, thiourea can induce variations in the electronic band structure and band-gap energy of the resulting film. Overall, the presence of sulfur and amine functional groups in the thiourea molecule allows it to interact with Cs_2SnI_6 films in multiple ways, exerting a significant influence on their optical and electronic properties.

To figure out the effect of thiourea as Lewis acid-base additive on Cs_2SnI_6 perovskite crystallization behavior and the corresponding modification on the surface state of CSI film, x-ray photoelectron spectroscopy (XPS) was performed. The XPS spectra of Cs_2SnI_6 films prepared with different amounts of thiourea are shown in Figs. 6(a)–6(c). The core-level spectra of Cs 3d, Sn 3d and I 3d can be assigned to two peaks respectively, Cs $3d_{5/2}$ (724.24 eV), Cs $3d_{3/2}$ (738.19 eV), Sn $3d_{5/2}$ (486.95 eV) and Sn $3d_{3/2}$ (496.26 eV) and I $3d_{5/2}$ (620.20 eV) and I $3d_{3/2}$ (632.11 eV). Compared to S_0, S_3 shows a shift of the element core level towards the lower binding energy.[35,36] It indicates the change of surrounding electron cloud density due to Lewis acid-base additive as a result of strong interaction between Sn^{4+} and thiourea molecule. As a result of Sn^{4+} and thiourea molecule interaction, a delocalized electron cloud could be formed which induces an interface dipole.[37]

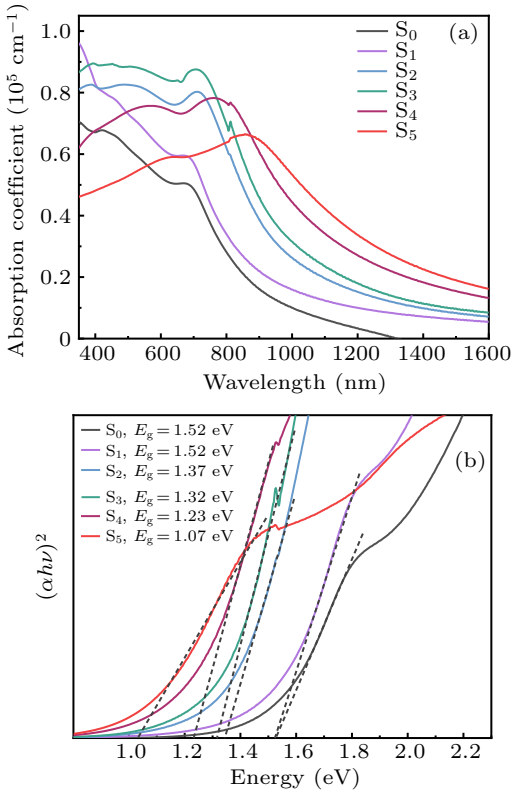


Fig. 5. (a) The UV–Vis spectra (a) and (b) Tauc plot of CSI film prepared with varying amounts of thiourea.

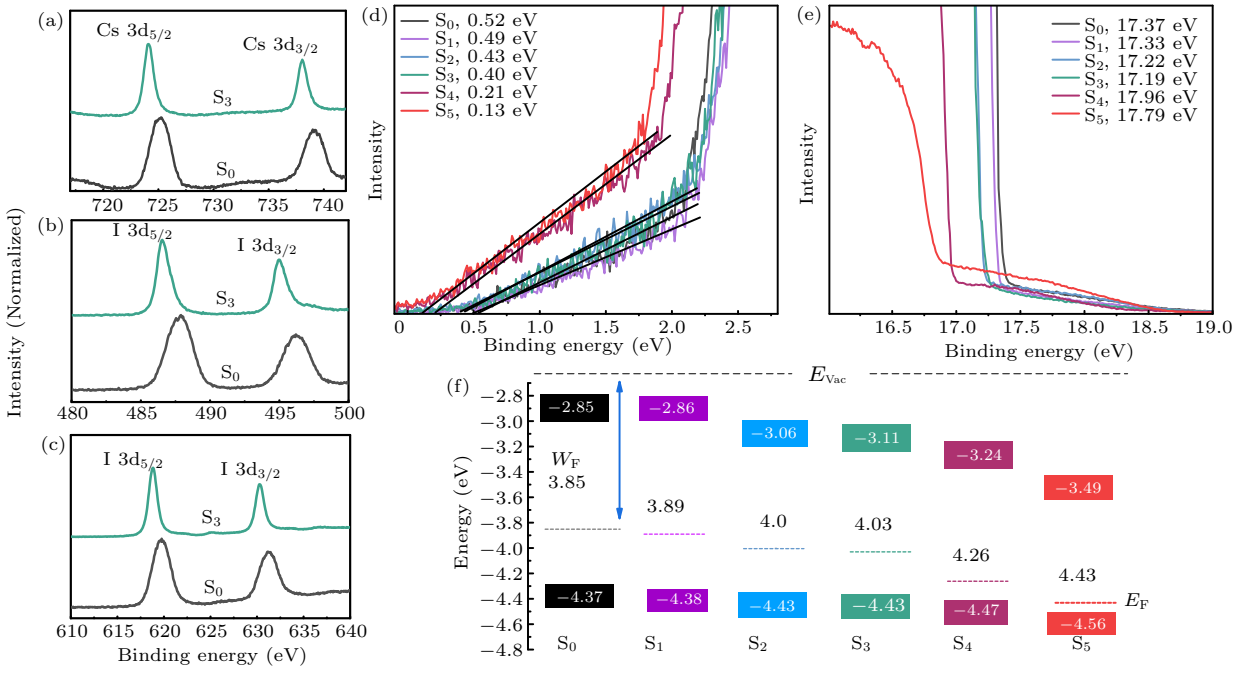


Fig. 6. (a)–(c) XPS core level spectra of Cs 3d, I 3d and Sn 3d of sample S_0 and S_3 films, (d) UPS plot of control and target Cs_2SnI_6 film: helium $I\alpha$ ($h\nu = 21.22$) (c) the secondary electron cutoff region, (e) the valance band region and (f) energy band diagram of samples prepared with varying amounts of thiourea concentration.

Thiourea, being a Lewis base, can donate electron pairs to the host material. Hence, the effect of thiourea on the electronic configuration is investigated using ultraviolet photoelectron spectroscopy (UPS), which provides the work function (WF) and valence band maximum (VBM) information as shown in Figs. 6(d) and 6(e). The work function determined from the secondary electron cutoff of samples S_0–S_5 increases from 3.85 eV to 4.43 eV, respectively, with respect to vacuum. Correspondingly, the Fermi level shifts downward from 0.52 eV to 0.13 eV relative to the valence band maximum (VBM). The incorporation of thiourea introduces additional energy states within the bandgap, which enhance the bonding overlap between Sn 5s and Sn 5p. Within the conduction band minimum (CBM), the heightened bonding overlap between Sn 5s and Sn 5p orbitals is potentially influenced by the reduction in Sn–I–Sn angles arising from the tilting of $[SnI_6]^{4-}$ octahedra. This geometric configuration leads to the prominence of Sn–I bonds over the distorted Sn–I–Sn angles, thereby facilitating a downward shift of the CBM position.[38,39] The Fermi level's movement towards the valence band maximum (VBM) indicates that the introduced energy states from thiourea concentration are located closer to the VBM. Based on derived bandgap and UPS studies, the band diagram is derived as shown in Fig. 6(f). Consequently, bandgap engineering becomes feasible as these altered energy states influence the charge carrier concentration and electronic behavior of the Cs_2SnI_6 thin film.

4. Conclusion

In summary, we prepared Cs_2SnI_6 thin film with pure crystalline orientation along the (222) plane and found the route to control the optical bandgap of the resultant film using direct solution-based coating process. We analyzed the effect of thiourea on crystalline orientation, tuning optical properties, film morphology, crystalline quality and phase purity of Cs_2SnI_6 film. It was found that with the increased amount of thiourea concentration, the resultant Cs_2SnI_6 film tends to orient along the (222) plane and is completely oriented in the case of a 0.42 mmol (S_3) thiourea concentration. The film morphology is optimized with increasing thiourea concentration and gives a better surface morphology at 0.42 mmol thiourea concentration. Such enhanced crystalline quality and surface morphology contribute to higher carrier concentration and mobility of 4.095 $\times 10^{15}$ cm^{-3} and 366 $cm^2/V{\cdot}s$, respectively. Besides, the optical bandgap varies from 1.52 eV to 1.07 eV along with an increased thiourea concentration showing a good control on bandgap and absorption coefficient. The current approach in this work using thiourea to obtain single-oriented pure phase Cs_2SnI_6 film with tunable optical properties shows potential to further diversify the application of solution-processed Cs_2SnI_6 lead-free perovskite.

Acknowledgements

Project supported by the National Natural Science Foundation of China (Grant Nos. 12174275, 62174113, 61874139, 61904201, and 11875088) and Guangdong Basic and Applied Basic Research Foundation (Grant No. 2019B1515120057). I am grateful to the Alliance of International Science Organization (ANSO) for financial support during my PhD studies at the Institute of Physics, CAS, University of the Chinese Academy of Sciences.

References

[1] Guo F, Lu Z, Mohanty D, Wang T, Bhat I B, Zhang S, Shi S, Washington M A, Wang G C and Lu T M 2017 *Mater. Res. Lett.* **5** 540
[2] Kapil G, Ohta T, Koyanagi T, Vigneshwaran M, Zhang Y, Ogomi Y, Pandey S S, Yoshino K, Shen Q, Toyoda T, Rahman M M, Minemoto T, Murakami T N, Segawa H and Hayase S 2017 *J. Phys. Chem. C* **121** 13092
[3] Qiu X, Cao B, Yuan S, Chen X, Qiu Z, Jiang Y, Ye Q, Wang H, Zeng H, Liu J and Kanatzidis M G 2017 *Sol. Energy Mater. Sol. Cells* **159** 227
[4] Ullah S, Wang J, Yang P, Liu L, Khan J, Yang S E, Xia T, Guo H and Chen Y 2021 *Sol. RRL* **5** 2000830
[5] Yang X, Wang Y, Jiang J, Li M, Tang Z, Cai H, Zhang F and Wu X 2020 *APL Mater.* **8** 021102
[6] Dang T C, Le H C, Pham D L, Nguyen S H, Nguyen T T O, Nguyen T T and Nguyen T D 2019 *J. Alloys Compd.* **805** 847
[7] Huang J, Dong C, Mei Y, Lu X, Yue G, Gao Y, Liu R, Zhang W and Tan F 2021 *J. Mater. Chem. C* **9** 14217
[8] Lee B, Krenselewski A, Baik S I, Seidman D N and Chang R P H 2017 *Sustain. Energy & Fuels* **1** 710
[9] Liu A, Zhu H, Reo Y, Kim M G, Chu H Y, Lim J H, Kim H J, Ning W, Bai S and Noh Y Y 2022 *Cell Rep. Phys. Sci.* **3** 100812
[10] Niu G, Yu H, Li J, Wang D and Wang L 2016 *Nano Energy* **27** 87
[11] Zhang G, Zhang J, Liao Y, Pan Z, Rao H and Zhong X 2022 *Chem. Eng. J.* **440** 135710
[12] Zhang Y, Ma Y, Wang Y, Zhang X, Zuo C, Shen L and Ding L 2021 *Adv. Mater.* **33** e200669
[13] Han X, Liang J, Yang J H, Soni K, Fang Q, Wang W, Zhang J, Jia S, Martí A A, Zhao Y and Lou J 2019 *Small* **15** 1901650
[14] Krishnaiah M, Kim S, Kumar A, Mishra D, Seo S G and Jin S H 2022 *Adv. Mater.* **34** 2109673
[15] Nairui X, Yehua T, Yali Q, Duoduo L and Ke-Fan W 2020 *Sol. Energy* **204** 429
[16] Shao D, Zhu W, Xin G, Liu X, Wang T, Shi S, Lian J and Sawyer S 2020 *J. Mat. Chem. C* **8** 1819
[17] Wang A, Yan X, Zhang M, Sun S, Yang M, Shen W, Pan X, Wang P and Deng Z 2016 *Chem. Mater.* **28** 8132
[18] Kumar J, Srivastava P and Bag M 2022 *Front. Chem.* **10** 842924
[19] Zheng D, Raffin F, Volovitch P and Pauporté T 2022 *Nat. Commun.* **13** 6655
[20] Konstantakou M, Perganti D, Falaras P and Stergiopoulos T 2017 *Crystals* **7** 291
[21] Yan Y, Yang Y, Liang M, Abdellah M, Pullerits T, Zheng K and Liang Z 2021 *Nat. Commun.* **12** 6603
[22] Hsieh C M, Liao Y S, Lin Y R, Chen C P, Tsai C M, Wei-Guang Diau E and Chuang S C 2018 *RSC Adv.* **8** 19610
[23] Ko S G, Ryu G I, Kim B, Cha G J, Ri J H, Sonu G S and Kim U C 2019 *Sol. Energy Mater. Sol. Cells* **196** 105
[24] Wang S, Ma Z, Liu B, Wu W, Zhu Y, Ma R and Wang C 2018 *Sol. RRL* **2** 1800034

[25] Yu S K, Xu N N, Jiang M, Weng Y G, Zhu Q Y and Dai J 2020 *Inorg. Chem.* **59** 15842
[26] Aming L and Yiyang S 2021 *J. Inorg. Mater.* **37** 691
[27] Kresse G and Furthmuller J 1996 *Phys. Rev. B* **54** 11169
[28] Blochl P E 1994 *Phys. Rev. B* **50** 17953
[29] Perdew J P, Burke K and Ernzerhof M 1996 *Phys. Rev. Lett.* **77** 3865
[30] Grimme S, Antony J, Ehrlich S and Krieg H 2010 *J. Chem. Phys.* **132** 154104
[31] Matussin S N, Rahman A and Khan M M 2022 *Front. Chem.* **10** 881518
[32] Wu B, Yuan H, Xu Q, Steele J A, Giovanni D, Puech P, Fu J, Ng Y F, Jamaludin N F, Solanki A, Mhaisalkar S, Mathews N, Roeffaers M B J, Grätzel M, Hofkens J and Sum T C 2019 *Nat. Commun.* **10** 484
[33] Ye S, Rao H, Zhao Z, Zhang L, Bao H, Sun W, Li Y, Gu F, Wang J, Liu Z, Bian Z and Huang C 2017 *J. Am. Chem. Soc.* **139** 7504
[34] Singh A, Najman S, Mohapatra A, Lu Y J, Hanmandlu C, Pao C W, Chen Y F, Lai C S and Chu C W 2020 *ACS App. Mater. Interfaces* **12** 32649
[35] Chen C, Li F, Zhu L, Shen Z, Weng Y, Lou Q, Tan F, Yue G, Huang Q and Wang M 2020 *Nano Energy* **68** 104313
[36] Wu Z, Jiang M, Liu Z, Jamshaid A, Ono L K and Qi Y 2020 *Adv. Energy Mater.* **10** 1903696
[37] Chen Q, Wang C, Li Y and Chen L 2020 *J. Am. Chem. Soc.* **142** 18281
[38] Mao L, Kennard R M, Traore B, Ke W, Katan C, Even J, Chabinyc M L, Stoumpos C C and Kanatzidis M G 2019 *Chem* **5** 2593
[39] Wu J, Liu S C, Li Z, Wang S, Xue D J, Lin Y and Hu J S 2021 *Natl. Sci. Rev.* **8** 047